Available online at www.eccomasproceedia.org
Eccomas Proceedia COMPDYN (2017) 1330-1346

ECCOMAS
Proceedia

COMPDYN 2017
6th ECCOMAS Thematic Conference on
Computational Methods in Structural Dynamics and Earthquake Engineering
M. Papadrakakis, M. Fragiadakis (eds.)
Rhodes Island, Greece, 15–17 June, 2017

MODELLING OF EVANESCENT AND PROPAGATING MODES IN HOMOGENIZED PHONONIC STRUCTURES IN FREQUENCY AND TIME DOMAINS

E. Rohan[1], **and R.Cimrman**[2]

[1]European Centre of Excellence, NTIS New Technologies for Information Society, Faculty of Applied Sciences, University of West Bohemia, Univerzitní 8, 306 14 Plze, Czech Republic
e-mail: rohan@kme.zcu.cz

[2]New Technologies Research Centre, University of West Bohemia, Univerzitní 8, 306 14 Plze, Czech Republic
e-mail: cimrman3@ntc.zcu.cz

Keywords: Phononic structures, band gaps, wave propagation, homogenization, spectral methods, time convolution

Abstract. *In the paper we deal with analytical and numerical methods for modelling phononic elastic structures subject to harmonic loading. The band gap prediction is based on the analysis of eigenvalues of the effective mass coefficients for a given frequency. Using a spectral decomposition method, the propagating and the evanescent modes can be distinguished in the frequency domain. We also developed a numerical scheme to simulate the wave response of the phononic 3D structures and plates, or beams in the time domain. Using the backward Laplace transformation, we obtain a model involving the intertia effects in terms of time convolutions, where the homogenized mass tensor serves as the convolution kernel. The aim of the reported modelling is to understand behaviour of the phononic structures subject to incident waves of frequencies falling in the partial (so-called weak) band gap intervals in which waves of certain polarizations cannot propagate. We discuss the issues related to the time-space discretization. Numerical examples of how homogenized phononic structures respond to a harmonic loading are presented.*

Peer-review under responsibility of the organizing committee of COMPDYN 2017.
doi: 10.7712/120117.5496.18256

1 INTRODUCTION

The phononic elastic solids, often called phononic crystals, are periodic structures made of components with large differences in their elastic coefficients, the soft phase being distributed in a form of inclusions embedded in a stiff matrix. For certain frequency ranges called band gaps, such elastic structures can effectively attenuate propagation of incident acoustic waves. Phononic structures attracted a considerable interest due to challenging application in design of metamaterial and smart devices, such as filters, resonators, and waveguides. In particular, plate structures, see e. g. [10] deserve a special attention.

This study presents a contribution to the very important area of the metamaterial engineering focused on structural vibration control, where plate and shell structures are used frequently. The phenomenon which is responsible for the band gaps occurrence is related to anti-resonance effects in periodic structures with large contrast in the elasticity, see [3]. Homogenization of such structures produces models of equivalent continua with indefinite or negative mass for certain frequencies, as reported in a number of papers [2, 1, 8]. Recetnly, the model developed in [2] was considered as bases for shape optimization of soft inclusuions periodically distributed in a stiff elastic matrix [9], cf. [5] in the context of piezoelectric phononic materials.

In paper [2], cf. [7], using the homogenization method and with the "dual porosity" type of the scaling ansatz applied in the inclusions, the following model of the phononic elastic solids occupying bounded domain Ω has been derived,

$$-\omega^2 \mathbb{M}(\omega^2)\boldsymbol{q} + \mathbb{K}\boldsymbol{q} = \boldsymbol{f}(\omega^2) \ , \quad \text{in } \Omega \ , \tag{1}$$

where $\omega \in \mathbb{R}$ is a fixed frequency, $\boldsymbol{q}(x) \in \mathbb{R}^d$ is the generalized displacements, $\mathbb{M} : \mathbb{R}^d \mapsto \mathbb{R}^d$ is the mass tensor (real symmetric, but possibly indefinite, depending on $\omega \in \mathbb{R}_+$) and $\mathbb{K}$ is the 2nd order (elliptic) differential operator, the stiffness. For the 3D elasticity problem (with $\boldsymbol{q} = \boldsymbol{u} = (u_i)$, $i = 1, 2, 3$) $\mathbb{K}$ attains the form $(\mathbb{K})_{ij} = -\partial_k D_{ikjl} \partial_j$ with D_{ikjl} being the usual symmetric positive definite elasticity tensor. Similar structure of the problem is retained by the model of homogenized Reissner-Mindlin phononic plates which was derived in [6]; the plate response $\boldsymbol{q}^T := [\boldsymbol{\theta}^T, w]$ expressed in terms of rotations $\boldsymbol{\theta} = (\theta_1, \theta_2)$ and deflections w is governed by (1), where,

$$\begin{aligned} \mathbb{K} &= \begin{bmatrix} -\frac{h^3}{3}\nabla \cdot \boldsymbol{\mathcal{D}} \nabla^S(\circ) + h\boldsymbol{\mathcal{G}}\circ & -h\boldsymbol{\mathcal{G}}\nabla\circ \\ h\nabla \cdot \boldsymbol{\mathcal{G}}\circ & -h\nabla \cdot \boldsymbol{\mathcal{G}}\nabla\circ \end{bmatrix} , \\ \mathbb{M}(\omega^2) &= \begin{bmatrix} \frac{h^3}{3}\boldsymbol{\mathcal{M}}(\omega^2) & \boldsymbol{0} \\ \boldsymbol{0}^T & h\mathcal{N}(\omega^2) \end{bmatrix} , \quad \boldsymbol{f}^T(\omega^2) = [\boldsymbol{0}^T, \mathcal{S}(\omega^2) f] \ , \end{aligned} \tag{2}$$

where ∇^S is the symmetric gradient, $\boldsymbol{\mathcal{D}}$ and $\boldsymbol{\mathcal{G}}$ are the elasticity parameters, while $\boldsymbol{\mathcal{M}}(\omega^2)$ and $\mathcal{N}(\omega^2)$ describe the frequency-dependent mass properties; we consider the transversal load by forces f only.

To predict the bang gap intervals for 2D, or 3D elastic structures, *i. e.* for $d = 2$, or $d = 3$, respectively, it is sufficient to compute and analyze eigenvalues of the homogenized mass $\mathbb{M}(\omega^2)$; when it becomes indefinite or negative definite, waves of certain polarizations cannot propagate. Relevancy of the homogenized model has been validated using the Bloch-Floquet modelling approach for large wave lengths in comparison with the period of heterogeneities [7]. Analysis of the wave response in phononic plates takes formally the same procedure, but is still not well understood; the band gaps structures are more complex especially in the Reissner-Mindlin plates, see [6]. In paper [4], we proposed a spectral decomposition method (SDM) which allows us to distinguish the propagating and the evanescent modes in the frequency domain.

In this paper, we aim to demonstrate an application of the SDM for modelling propagating and attenuated modes in plate structures. Analytical solution is obtained for the Timoshenko beam, *i. e.* for a 1D problem with two degrees of freedom corresponding to the beam rotation and deflection. Then we consider solution of an elastodynamic problem governed by (1) in the time domain; in particular we explain the time discretization of the model involving time convolutions.

2 SPECTRAL DECOMPOSITION METHOD (SDM)

The purpose of solving (1) using the spectral based method is to separate the the wave and evanescent parts of the solution, when frequencies ω of periodic loading fall in band gaps, so that a negative eigenvalue of $\mathbb{M}(\omega^2)$ exists. We only consider ω such that $\det(-\omega^2\mathbb{M}(\omega^2) + \mathbb{K}) \neq 0$ and disregard loading with resonance frequencies. In order to separate the positive and the negative part of the effective mass operator, we compute the eigenvalues and eigenvectors $(\lambda^r, \boldsymbol{p}^r)$ satisfying

$$\mathbb{M}\boldsymbol{p}^r = \lambda^r \boldsymbol{p}^r \ , \quad |\boldsymbol{p}^r|^2 = (\boldsymbol{p}^r)^T \boldsymbol{p}^r = 1 \ , \quad r = 1, 2, \dots d \ , \tag{3}$$

and define $\boldsymbol{P} = [\boldsymbol{p}^1, \dots, \boldsymbol{p}^d]$ and $\boldsymbol{\Lambda} = \mathrm{diag}(\lambda^1, \dots, \lambda^d)$, obviously $\boldsymbol{P}^T\boldsymbol{P} = \boldsymbol{I}$. This allows us to introduce the following transformation. First we define $\mathbb{A} := \boldsymbol{P}^T\mathbb{K}\boldsymbol{P}$, then using $\boldsymbol{b}(\omega^2) = \boldsymbol{P}^T\boldsymbol{f}(\omega^2)$ and assuming space-independent homogenized coefficients (perfectly periodic structures), problem (1) can be written, as follows: Since the spectral decompositions relies on projections of eigenfunctions, the weak formulations is needed. Using the the inner product $\langle \cdot, \cdot \rangle_\Omega$, the weak form of (1) becomes

$$-\omega^2 \langle \boldsymbol{\Lambda}\boldsymbol{\xi}, \boldsymbol{\zeta} \rangle_\Omega + \langle \mathbb{A}\boldsymbol{\xi}, \boldsymbol{\zeta} \rangle_\Omega = \langle \boldsymbol{b}(\omega^2), \boldsymbol{\zeta} \rangle_\Omega \ , \quad \text{for all } \boldsymbol{\zeta} \in W_0(\Omega) \ , \tag{4}$$

where $W_0(\Omega)$ is the space of test functions associated with the admissibility set $W(\Omega) := \boldsymbol{P}^T Q(\Omega)$, i.e. $\boldsymbol{\xi} \in W(\Omega) \Leftrightarrow \boldsymbol{\xi} = \boldsymbol{P}^T\boldsymbol{q}$ and $\boldsymbol{q} \in Q(\Omega)$. In the following we shall consider only the case $Q(\Omega) = Q_0(\Omega)$, consequently $W(\Omega) = W_0(\Omega)$.

2.1 Spectral decomposition – general scheme

Matrix $\mathbb{M}(\omega^2)$ can be indefinite, so that $\boldsymbol{\Lambda}$, which also depends on ω, can be split into positive and negative parts, denoted $\boldsymbol{\Lambda}^+$ and $\boldsymbol{\Lambda}^-$, respectively,

$$\boldsymbol{\Lambda} = \boldsymbol{\Lambda}^+ + \boldsymbol{\Lambda}^- \ , \quad \boldsymbol{z}^T\boldsymbol{\Lambda}^+\boldsymbol{z} \geq 0 \ , \quad \boldsymbol{z}^T\boldsymbol{\Lambda}^-\boldsymbol{z} < 0 \quad \forall \boldsymbol{z} \in \mathbb{R}^d \ , \quad |\boldsymbol{z}| = 1 \ . \tag{5}$$

We can now consider two uncoupled eigenvalue problems, although presented below in a generic form as one problem (6) for both the alternatives $\pm$, which provide two complementary bases $\{\boldsymbol{\zeta}^+\}$ and $\{\boldsymbol{\zeta}^-\}$, such that $\langle \boldsymbol{\Lambda}\boldsymbol{\zeta}^+, \boldsymbol{\zeta}^- \rangle_\Omega = 0$. (For the sake of brevity we shall use a compound notation, e.g. $a^\pm = \pm b^\pm c^\mp$ means $a^+ = b^+c^-$ and $a^- = -b^-c^+$).

Find $\boldsymbol{\zeta}^\pm \in W_0(\Omega)$ normalized by $\langle \boldsymbol{\Lambda}^\pm\boldsymbol{\zeta}^\pm, \boldsymbol{\zeta}^\pm \rangle_\Omega = \pm 1$, and $\mu^\pm \in \mathbb{R}$, such that

$$\left\{ \begin{array}{rcll} \langle \mathbb{A}\boldsymbol{\zeta}^\pm, \boldsymbol{\eta} \rangle_\Omega - \mu^\pm \langle \boldsymbol{\Lambda}^\pm\boldsymbol{\zeta}^\pm, \boldsymbol{\eta} \rangle_\Omega + \left\langle \boldsymbol{\Lambda}^\mp\tilde{\boldsymbol{\xi}}^\pm, \boldsymbol{\eta} \right\rangle_\Omega &=& 0 \ , & \forall \boldsymbol{\eta} \in W_0(\Omega) \ , \\ \left\langle \boldsymbol{\Lambda}^\mp\tilde{\boldsymbol{\theta}}, \boldsymbol{\zeta}^\pm \right\rangle_\Omega &=& 0 \ , & \forall \tilde{\boldsymbol{\theta}} \in W_0(\Omega) \ , \end{array} \right. \tag{6}$$

where $\tilde{\boldsymbol{\xi}}^\pm$ are multipliers. We recall that the eigenvalues have their signs: $\mu^+ > 0$ while $\mu^- < 0$.

It can be seen that $W_0(\Omega) = \mathrm{span}\{\boldsymbol{\zeta}_r^+\}_r \oplus \mathrm{span}\{\boldsymbol{\zeta}_s^-\}_s$ Consequently the multipliers are in the complementary subspaces, thus, $\tilde{\boldsymbol{\xi}}^+ \in \mathrm{span}\{\boldsymbol{\zeta}_k^-\}_k$, and $\tilde{\boldsymbol{\xi}}^- \in \mathrm{span}\{\boldsymbol{\zeta}_l^+\}_l$. Obviously there is one multiplier for each eigenfunction: let $(\mu_r^+, \boldsymbol{\zeta}_r^+)$ and $(\mu_s^-, \boldsymbol{\zeta}_s^-)$ be the eigen-pairs satisfying (6) with multipliers $\tilde{\boldsymbol{\xi}}_r^+$ and $\tilde{\boldsymbol{\xi}}_s^-$, respectively, then $\tilde{\boldsymbol{\xi}}_r^+ = \sum_k \gamma_k^{+r} \boldsymbol{\zeta}_k^-$, and $\tilde{\boldsymbol{\xi}}_s^- = \sum_l \gamma_l^{-s} \boldsymbol{\zeta}_l^+$. Using (6), coefficients γ_k^{+r} can be computed, as follows:

$$\gamma_s^{+r} = \left\langle \mathbb{A}\boldsymbol{\zeta}_r^+, \boldsymbol{\zeta}_s^- \right\rangle_\Omega = \left\langle \mathbb{A}\boldsymbol{\zeta}_s^-, \boldsymbol{\zeta}_r^+ \right\rangle_\Omega = -\gamma_r^{-s} \,. \tag{7}$$

To solve the wave propagation problem, in (4) where we substitute $\boldsymbol{\xi} = \boldsymbol{\xi}^+ + \boldsymbol{\xi}^-$ with $\boldsymbol{\xi}^+ = \sum_r c_r^+ \boldsymbol{\zeta}_r^+$ and $\boldsymbol{\xi}^- = \sum_s c_s^- \boldsymbol{\zeta}_s^-$. The applied force coefficients f_k^+ and f_k^- are evaluated as the following projections:

$$f_k^+ = \left\langle \boldsymbol{b}(\omega^2), \boldsymbol{\zeta}_k^+ \right\rangle_\Omega \,, \qquad f_l^- = \left\langle \boldsymbol{b}(\omega^2), \boldsymbol{\zeta}_l^- \right\rangle_\Omega \,. \tag{8}$$

By virtue of the properties of the eigenproblem solutions, see (6),we obtain a coupled system of linear algebraic equations for coefficients c_r^+ and c_s^-; it can be presented using the matrix form:

$$\begin{bmatrix} \mathrm{diag}[\mu_r^+ - \omega^2]_{rr} & [\gamma_s^{+r}]_{rs} \\ ([\gamma_s^{+r}]_{rs})^T & \mathrm{diag}[\omega^2 - \mu_s^-]_{ss} \end{bmatrix} \begin{bmatrix} (c_r^+)_r \\ (c_s^-)_s \end{bmatrix} = \begin{bmatrix} (f_r^+)_r \\ (f_s^-)_s \end{bmatrix} . \tag{9}$$

To compute numerical solutions, we consider finite subspaces $\mathrm{span}\{\boldsymbol{\zeta}_r^+\}_{r\le\bar{r}}$ and $\mathrm{span}\{\boldsymbol{\zeta}_s^-\}_{s\le\bar{s}}$ generated by the finite set of eigenfunctions. Then $(c_r^+)_r$ is the column matrix with rows indices $r \in [1, \bar{r}]$, the analogous notation holds for $(c_s^-)_s$; similarly $[\,]_{rs}$ is the matrix with rows/column indices ranging $r \in [1, \bar{r}]$ and $s \in [1, \bar{s}]$.

We may conclude that the part $\boldsymbol{\xi}^+$ represents a wave response, whereas $\boldsymbol{\xi}^-$ describes evanescent modes which are attenuated with spatial coordinate measuring the distance from the excitation, or loading source. Therefore, we keep only the positive part of the solution $\boldsymbol{\xi}^+ = \sum_r c_r^+ \boldsymbol{\zeta}_r^+$ which yields $\boldsymbol{q} = \boldsymbol{P}\boldsymbol{\xi}^+$ as the response in the physical coordinates, such as displacements.

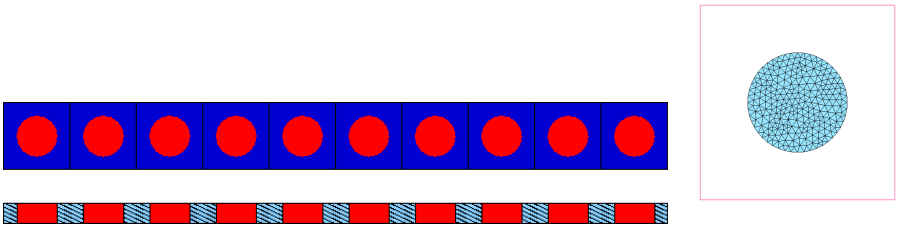

Figure 1: Left: A phononic beam made of soft cylindric inclusions in stiff elastic matrix. View from the top and view of the longitudinal section. Right: The representative cell defined on the plate, or beam mid-plane.

2.2 Timoshenko beams – analytic solutions using the SDM

We illustrate how the SDM methods is applied to analyze wave response of the phononic Timoshenko beam. The model equations can be obtained from the model of the Reissner-Mindlin plate. The coordinate $x \in]0, L[$ spans the beam axial position. The rotations $\theta(x)$ and deflection $w(x)$ (in one plane) of the beam satisfy the following equations,

$$\begin{aligned} -\omega^2 \frac{h^3}{3} \mathcal{M}(\omega^2)\theta - \frac{h^3}{3}\mathcal{D}\theta'' - h\mathcal{G}(w' - \theta) &= \hat{g} \,, \\ -\omega^2 h \mathcal{N}(\omega^2) w - h\mathcal{G}(w'' - \theta') &= \hat{\sigma} \,, \end{aligned} \tag{10}$$

where $(\,)' = \partial/\partial x$, the coefficients $\mathcal{M}(\omega^2)$, $\mathcal{N}(\omega^2)$, $\mathcal{D}$ and $\mathcal{G}$ are obtained in the same way as for the plate model with few modifications. Functions $\hat{g}$ and $\hat{\sigma}$ describing generalized forces are established below. The boundary conditions describe a kinematic loading of a cantilever beam: at $x = 0$ it is clamped, while at $x = L$ vertical harmonic displacement is prescribed, thus, we consider

$$w(0) = 0\ , \quad w(L) = \bar{w}\ , \quad \theta(0) = 0\ , \quad \theta'(L) = 0\ , \tag{11}$$

where $\bar{w}$ is the amplitude of harmonic oscillations. Note that the last condition means zero bending moment at $x = L$. Further, we introduce the split $w(x) = \tilde{w}(x) + \hat{w}(x)$, where $\hat{w}(x) = \bar{w}\frac{x}{L}$ and the following functions:

$$\begin{aligned} \hat{g}(x) &= h\mathcal{G}(\hat{w}(x))' = h\mathcal{G}\frac{\bar{w}}{L}\ , \\ \hat{\sigma}(x) &= \omega^2\mathcal{N}(\omega)\hat{w}(x) = \omega^2\mathcal{N}(\omega)\frac{\bar{w}}{L}x\ . \end{aligned} \tag{12}$$

In what follows, for the sake of simplicity we denote $w(x) := \tilde{w}(x)$. We define $\boldsymbol{\xi} = (\theta, w)$ and the differential operator $\mathbb{A}$, such that

$$\mathbb{A}\boldsymbol{\xi} = -\begin{pmatrix} \frac{h^3}{3}\mathcal{D}(\bullet)'' - h\mathcal{G}\ , & h\mathcal{G}(\bullet)' \\ -h\mathcal{G}(\bullet)'\ , & h\mathcal{G}(\bullet)'' \end{pmatrix}\begin{pmatrix} \xi_1 \\ \xi_2 \end{pmatrix}\ . \tag{13}$$

Consequently, (10) can be written in the following form:

$$-\omega^2\boldsymbol{\Lambda}(\omega^2)\boldsymbol{\xi} + \mathbb{A}\boldsymbol{\xi} = \boldsymbol{f}\ , \tag{14}$$

where $\boldsymbol{f} = (\hat{g}, \hat{\sigma})$ and $\boldsymbol{\Lambda}(\omega^2) = \mathrm{diag}(\mathcal{M}(\omega^2), \mathcal{N}(\omega^2)) = \mathrm{diag}(\lambda_1, \lambda_2)$. Note that $\boldsymbol{\Lambda}(\omega^2) = \mathbb{M}(\omega^2)$ is diagonal, thus the problem (3) is trivial, $\boldsymbol{P} = \boldsymbol{I}$.

Since the mass coefficients $\mathcal{M}(\omega^2)$ and $\mathcal{N}(\omega^2)$ can be negative, the following cases of $\boldsymbol{\Lambda}(\omega^2)$ with respect to an imposed frequency ω should be distinguished (the equality cases are disregarded):

1. $\mathcal{M}(\omega^2) > 0$ and $\mathcal{N}(\omega^2) < 0$, or
2. $\mathcal{M}(\omega^2) < 0$ and $\mathcal{N}(\omega^2) > 0$, or
3. $\mathcal{M}(\omega^2) < 0$ and $\mathcal{N}(\omega^2) < 0$, or
4. $\mathcal{M}(\omega^2) > 0$ and $\mathcal{N}(\omega^2) > 0$.

Hence, the case 1 and 2, thus, representing the partial bangaps, lead to similar problems, the vave propagation is unlimited in case 4, while no waves can propagate in case 3, thus, representing the full band gap. Here, we consider $\mathcal{M}(\omega^2) > 0$ and $\mathcal{N}(\omega^2) < 0$, *i. e.* $\lambda_1 > 0$ and $\lambda_2 < 0$. We can follow the general procedure based on the eigenvalue problems (6). Thus, we have two problems, where the Lagrange multipliers are denoted by $\boldsymbol{z}^{\pm} = (z_1^{\pm}, z_2^{\pm})$,

1. Find $\boldsymbol{\zeta}^+ \in W_0(0, L)$, multiplier z_2^+, and $\mu^+ \in \mathbb{R}$ such that

$$\mathbb{A}\boldsymbol{\zeta}^+ + \begin{pmatrix} -\mu^+\lambda_1\zeta_1^+ \\ \lambda_2 z_2^+ \end{pmatrix} = \boldsymbol{0}\ , \qquad \zeta_2^+ = 0\ . \tag{15}$$

2. Find $\boldsymbol{\zeta}^- \in W_0(0,L)$, multiplier z_1^-, and $\mu^- \in \mathbb{R}$ such that

$$\mathbb{A}\boldsymbol{\zeta}^- + \begin{pmatrix} \lambda_1 z_1^- \\ -\mu^- \lambda_2 \zeta_2^- \end{pmatrix} = \boldsymbol{0} \,, \qquad \zeta_1^- = 0 \,. \tag{16}$$

Note that neither of the multipliers z_1^+, z_2^- is involved in the problem. Due to (13), (15) reduces to

$$\begin{aligned} -(\zeta_1^+)'' &= m^+ \zeta_1^+ \,, \quad m^+ = (\mu^+ \mathcal{M}(\omega^2) - h\mathcal{G})3/(\mathcal{D}h^3) \,, \\ \mathcal{N}(\omega^2) z_2^+ &= -h\mathcal{G}(\zeta_1^+)' \,, \end{aligned} \tag{17}$$

whereas (16) yields

$$\begin{aligned} -(\zeta_2^-)'' &= m^- \zeta_2^- \,, \quad m^- = \mu^- \mathcal{N}(\omega^2)/(h\mathcal{G}) \,, \\ \mathcal{M}(\omega^2) z_1^- &= h\mathcal{G}(\zeta_2^-)' \,. \end{aligned} \tag{18}$$

Recalling the boundary conditions (11), we obtain the following two bases:

1. $\{\boldsymbol{\zeta}^{+k}\}$ for $k = 1, 2, \ldots$, where $\boldsymbol{\zeta}^{+k} = (\zeta_1^{+k}, \zeta_2^{+k})$ is such that,

$$\begin{aligned} \zeta_1^{+k} &= \nu^{+k} \sin\left(\frac{2k-1}{2L}\pi x\right) \,, \quad \zeta_2^{+k} = 0 \,, \\ \mu^{+k} &= \mathcal{M}(\omega^2)^{-1} \left(\frac{h^3}{3}\mathcal{D}\left(\frac{2k-1}{2L}\pi\right)^2 + h\mathcal{G}\right) \,, \end{aligned} \tag{19}$$

   where $\nu^{+k} = \sqrt{2/(|\lambda_1|L)}$.

2. $\{\boldsymbol{\zeta}^{-k}\}$ for $k = 1, 2, \ldots$, where $\boldsymbol{\zeta}^{-k} = (\zeta_1^{-k}, \zeta_2^{-k})$ is such that,

$$\begin{aligned} \zeta_2^{-k} &= \nu^{-k} \sin\left(\frac{k\pi x}{L}\right) \,, \quad \zeta_1^{-k} = 0 \,, \\ \mu^{-k} &= \frac{h\mathcal{G}}{\mathcal{N}(\omega^2)} \left(\frac{k\pi}{L}\right)^2 \,, \end{aligned} \tag{20}$$

   where $\nu^{-k} = \sqrt{2/(|\lambda_2|L)}$.

The projections of $\boldsymbol{f}$ into the two bases yield:

$$\begin{aligned} f^{+k} &= \int_0^L (\hat{g}\zeta_1^{+k} + \hat{\sigma}\zeta_2^{+k}) = h\mathcal{G}\nu^{+k} \frac{2\bar{w}}{(2k-1)\pi} \,, \\ f^{-k} &= \int_0^L (\hat{g}\zeta_1^{-k} + \hat{\sigma}\zeta_2^{-k}) = \omega^2 \mathcal{N}(\omega^2)\nu^{-k} \frac{\bar{w}L}{k\pi}(-1)^{k+1} \,. \end{aligned} \tag{21}$$

Further we need the mixt projections in the energy product, see (7). For the given bases (19) and (20), we obtain:

$$\begin{aligned} \int_0^L (\zeta_1^{+i})' \zeta_2^{-k} &= \frac{2i-1}{2L}\pi \int_0^L \cos\left(\frac{2i-1}{2L}\pi x\right) \sin\left(\frac{k\pi x}{L}\right) \nu^{+i}\nu^{-k} \\ &= -\frac{2k(2i-1)}{(2i-1)^2 - (2k)^2} \nu^{+i}\nu^{-k} \,. \end{aligned} \tag{22}$$

Now the coefficients γ_s^{+r} can be computed:

$$\begin{aligned}\gamma_s^{+r} &= \int_0^L [\mathbb{A}\boldsymbol{\zeta}^{+r}]\cdot\boldsymbol{\zeta}^{-s} = \mu^{+r}\int_0^L [\boldsymbol{\Lambda}^{+}\boldsymbol{\zeta}^{+r}]\cdot\boldsymbol{\zeta}^{-s} + \int_0^L [\boldsymbol{\Lambda}^{-}\boldsymbol{z}^{+r}]\cdot\boldsymbol{\zeta}^{-s}\\ &= h\mathcal{G}\frac{2s(2r-1)}{(2r-1)^2-(2s)^2}\nu^{+r}\nu^{-s}\,.\end{aligned} \tag{23}$$

We assume the solution of (14) decomposed into positive and negative parts,

$$\boldsymbol{\xi} = \boldsymbol{\xi}^{+} + \boldsymbol{\xi}^{-}\,,\ \text{where}\quad \boldsymbol{\xi}^{\pm} = \sum_k c^{\pm k}\boldsymbol{\zeta}^{\pm k}\,. \tag{24}$$

Using the general procedure, see (9), and taking a finite number of modes $\bar{k}$, the following equations for $c_k^{\pm}$, $k = 1, 2, \ldots, \bar{k}$ are obtained,

$$\begin{aligned}(\mu^{+k}-\omega^2)c_k^{+} + \sum_{r=1}^{\bar{k}}\gamma_r^{+k}c_r^{-} &= f^{+k}\,,\\ (\mu^{-k}-\omega^2)c_k^{-} - \sum_{s=1}^{\bar{k}}\gamma_s^{-k}c_s^{+} &= f^{-k}\,.\end{aligned} \tag{25}$$

Although both (c_r^{+}) and (c_s^{-}) must be computed, the propagating waves with frequencies in (the partial) band gaps are given in terms of c_r^{+} only. Due to the splitting, we can distinguish the propagating part of the solution from the part associated with the evanescent modes expressed in terms of c_r^{-}.

$$\begin{aligned}\text{propagating modes:}\quad \boldsymbol{\xi}^{+} &= \sum_{r=1}^{\bar{k}} c_r^{+}\boldsymbol{\zeta}^{+k}\,,\\ \text{evanescent modes:}\quad \boldsymbol{\xi}^{-} &= \sum_{r=1}^{\bar{k}} c_r^{-}\boldsymbol{\zeta}^{-k}\,,\end{aligned} \tag{26}$$

where $\boldsymbol{\xi}^{+} = (\theta^{+}, 0)$, while $\boldsymbol{\xi}^{-} = (0, w^{-})$. Therefore, in the given case, only waves of rotations can propagate, while the deflection waves are attenuated.

2.3 Numerical illustration

The beam can be considered as a special form of the plate, therefore the homogenized coefficients, namely $\mathcal{M}(\omega^2)$, $\mathcal{N}(\omega^2)$, $\mathcal{D}$ and $\mathcal{G}$ are computed using formuale given in [6] with the material parameters given at the level periodic heterogeneity in Tab. 1, whereby the periodic structure is generated by cylindrical inclusions which are defined by the circle in the 2D reference periodic cell, see Fig. 1.

The SDM approach to the wave response analysis for loading with frequencies in partial band gaps is illustrated in Fig. 2, where the oscillating angle $\theta = \xi_1^{+}$ and the evanescent deflection $w = \xi_2^{-}$ are depicted for 3 selected frequencies for which $\mathcal{M}(\omega) > 0$, while $\mathcal{N}(\omega) < 0$.

The problem given equation (14), can be solved numerically using the finite element method. Thus we can obtain an "overall response" of the harmonically loaded Timoshenko beam.As a result we obtain space-frequency maps of amplitudes, as in Fig. 3. For the given structure and material parameters, the band gap of the deflection modes, *i. e.* $\mathcal{N}(\omega) < 0$, starts at $\omega = 9698$ Hz (red line). In Fig. 3, the effect of changing the frequency is clearly visible.

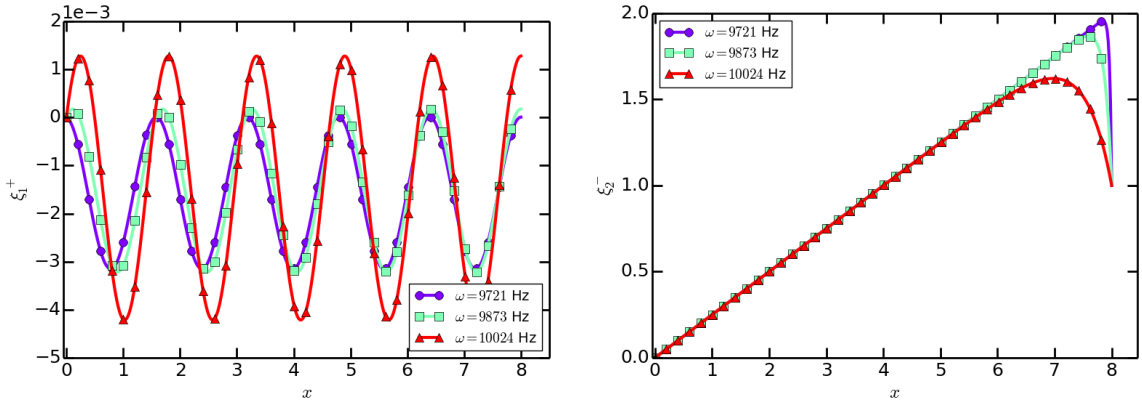

Figure 2: The SDM method employed to distinguish propagating (left) and evanescent (right) modes of the rotations θ and deflections w, respectively, in the Timoshenko beam ????????.

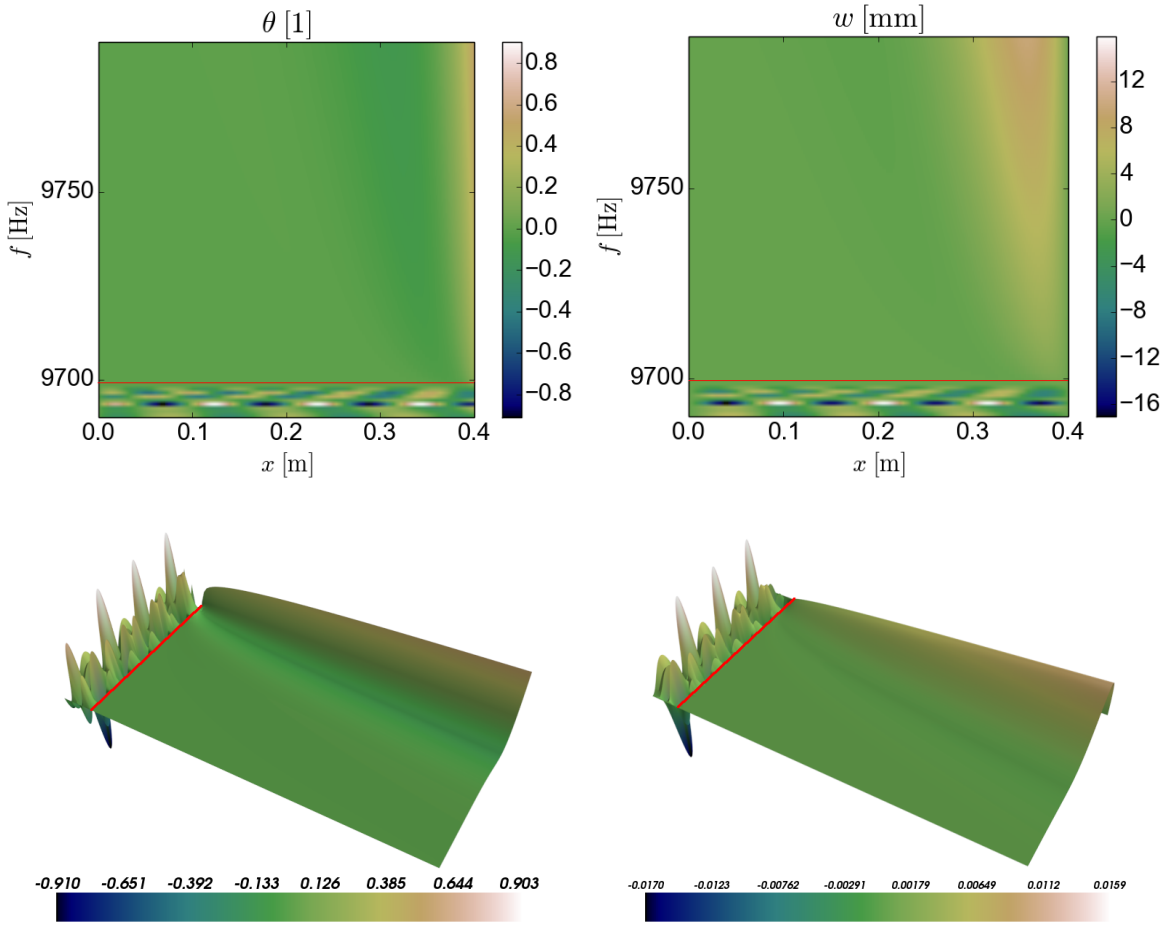

Figure 3: Space-frequency maps of amplitudes. Top row: 2D view, bottom row: 3D view, left column: the rotation $\theta(f, x)$ amplitude, right column: the deflection $w(f, x)$ amplitude. The red line marks the start of the $\mathcal{N}(\omega)$-related band gap.

3 NUMERICAL SIMULATIONS IN TIME DOMAIN

The frequency response of phononic structures described by the homogenized model (1) and analysed using the SDM described above provides the "static" monochromatic response to the imposed loading. For understanding the behaviour of these structures for prescribed initial conditions, we consider initial-boundary value (IBV) problems for phononic structures governed by (1) subject to the inverse Fourier transformation $\mathcal{F}^{-1}$ yilding time convolutions with kernel $\mathcal{F}^{-1}(\mathbb{M}(\omega^2))(t)$. Below we introduce the IBV problem for 3D homogenized phononic solids, then we explain the time discretization of the convolution integrals on an example of the Timoshenko beam which was treated in the preceding section using the SDM method.

3.1 Inverse Fourier transformation

For a 3D phononic solid, the general model (1) attains a simple form,

$$-\omega^2 \boldsymbol{\mathcal{M}}(\omega^2)\boldsymbol{u} - \nabla\cdot\mathbb{D}\nabla^S\boldsymbol{u} = \boldsymbol{\mathcal{R}}(\omega^2)\tilde{\boldsymbol{f}}\ , \tag{27}$$

where $\boldsymbol{\mathcal{R}}(\omega^2)$ is the tensor of applied volume forces, see [7]; when gravity forces are considered, thus, related to the mass density, $\boldsymbol{\mathcal{R}}(\omega^2) = \boldsymbol{\mathcal{M}}(\omega^2)$. To present the model in the time domain, the homogenized mass $\boldsymbol{\mathcal{M}}(\omega^2)$ must be transformed by the inverse Fourier transformation. In general, the effective mass in the frequency domain is given by

$$\boldsymbol{\mathcal{M}}(\omega^2) = \overline{\rho}\boldsymbol{I} - \sum_r \frac{\omega^2}{\omega^2-\lambda^r}\boldsymbol{m}^r\otimes\boldsymbol{m}^r\ , \tag{28}$$

where $\overline{\rho}$ is the mean density and $\boldsymbol{m}^r$ is the eigenmomentum associated with the eigenvalue λ^r. The inverse Fourier transformation $\mathcal{F}^{-1}(\boldsymbol{\mathcal{M}}(\omega^2)) = \boldsymbol{M}(t)$ yields the following result,

$$\mathcal{F}^{-1}\left(\boldsymbol{\mathcal{M}}(\omega^2)\right) = \sqrt{2\pi}\overline{\rho}\boldsymbol{I}\delta(t) - \sqrt{2\pi}\sum_r\left(\delta(t) - \frac{\sqrt{\lambda^r}}{2}\sin(\sqrt{\lambda^r}t)\right)\boldsymbol{m}^r\otimes\boldsymbol{m}^r\ , \tag{29}$$

hence, we may introduce

$$\begin{aligned}
\boldsymbol{M}(t) &= \overline{\boldsymbol{M}}\delta(t) + \sum_r \sin(\sqrt{\lambda^r}t)\widetilde{\boldsymbol{M}}^r\ ,\\
\text{where}\quad \overline{\boldsymbol{M}} &= \sqrt{2\pi}\left(\overline{\rho}\boldsymbol{I} - \sum_r \boldsymbol{m}^r\otimes\boldsymbol{m}^r\right)\ ,\\
\widetilde{\boldsymbol{M}}^r &= \sqrt{2\pi}\frac{\sqrt{\lambda^r}}{2}\boldsymbol{m}^r\otimes\boldsymbol{m}^r\ .
\end{aligned} \tag{30}$$

Now the elasto-dynamic equation for a 3D phononic continuum in the time domain reads as

$$\int_0^t \boldsymbol{M}(t-s)\ddot{\boldsymbol{u}}(s)\mathrm{d}s - \nabla\cdot\mathbb{D}\boldsymbol{e}(\boldsymbol{u}) = \int_0^t \boldsymbol{R}(t-s)\tilde{\boldsymbol{f}}(s)\mathrm{d}s\ , \tag{31}$$

where we assume a "gentle start" conditions, i.e. $\boldsymbol{u}(t) = \dot{\boldsymbol{u}}(t) = \ddot{\boldsymbol{u}}(t) = 0$ for all $t \le 0$. By causality, the integration applies between $s = 0$ and $s = t$ (and not $+\infty$). In general, the convolution kernel $\boldsymbol{R}$ has a similar structure as $\boldsymbol{M}$, see the remark above.

3.2 Phononic beam model – time domain

By virtue of (30), for the phononic beam model (10), the following convolution kernels are defined:

$$\mathcal{M}(t) = \overline{\mathcal{M}}\delta(t) + \sum_r \sin(\alpha^r t)\widetilde{\mathcal{M}}^r \,, \qquad \mathcal{N}(t) = \overline{\mathcal{N}}\delta(t) + \sum_r \sin(\beta^r t)\widetilde{\mathcal{N}}^r \,, \tag{32}$$

$$\overline{\mathcal{M}} = \sqrt{2\pi}(\overline{\rho} - \sum_r (a^r)^2) \,, \qquad \overline{\mathcal{N}} = \sqrt{2\pi}(\overline{\rho} - \sum_r (b^r)^2) \,, \tag{33}$$

$$\widetilde{\mathcal{M}}^r = \sqrt{2\pi}\frac{\alpha^r}{2}(a^r)^2 \,, \qquad \widetilde{\mathcal{N}}^r = \sqrt{2\pi}\frac{\beta^r}{2}(b^r)^2 \,, \tag{34}$$

where a^r and b^r are the eigenmomenta computed for the r-th mode, and $\alpha^r = \sqrt{\lambda^r}$, $\beta^r = \sqrt{\mu^r}$ are eigenfrequencies associated with the rotational and deflection modes of the Timoshenko beam model.

We now introduce the phononic beam equations in the time domain. For the sake of simplicity, still the same notation (θ, w) is used for the functions of time. The boundary conditions are as in (11). On $x = L$, the deflections $\overline{w}(1 - \cos\omega t)$ are prescribed, so that for $x \in]0, L[$ they attain the following decomposed form,

$$w(t,x) = \tilde{w}(t,x) + \hat{w}(t,x) \,, \qquad \text{where } \hat{w}(t,x) := \overline{w}\frac{x}{L}(1 - \cos\omega t) \,. \tag{35}$$

Further we define (see (12))

$$\begin{aligned} \phi(t) &= h\mathcal{G}\frac{\overline{w}}{L}(1 - \cos\omega t) \,, \\ f(t,x) &= -h\int_0^t \mathcal{N}(t-s)\ddot{\hat{w}}(s,x)\mathrm{d}s = -h\omega^2\frac{\overline{w}x}{L}\int_0^t \mathcal{N}(t-s)\cos(\omega t)\mathrm{d}s \,. \end{aligned} \tag{36}$$

We shall consider the following problem: Find $(\theta, w)(t,x)$ satisfying for $(t,x) \in]0,T]\times]0,L[$, $T > 0$ the following equalities

$$\begin{aligned} \frac{h^3}{3}\int_0^t \mathcal{M}(t-s)\ddot{\theta}(s)\mathrm{d}s - \frac{h^3}{3}\mathcal{D}\theta'' - h\mathcal{G}(\tilde{w}' - \theta) &= \phi(t) \,, \\ h\int_0^t \mathcal{N}(t-s)\ddot{\tilde{w}}(s)\mathrm{d}s - h\mathcal{G}(\tilde{w}'' - \theta') &= f(t,x) \,, \end{aligned} \tag{37}$$

such that $\tilde{w}(t,0) = \tilde{w}(t,L) = \theta(t,0) = 0$ for $t > 0$ and the initial conditions $\theta(0,x) = \tilde{w}(0,x) = 0$.

To compute numerical solutions of this problem, we use a semidiscrtization in time using a sheme which is described in subsequent sections, and use the finite element method for discretization in space of the weak formulation. For this, we need the space $W_0(0,L) = \{(\psi, z) \in [H^1(0,L)]^2,\ \psi(0) = z(0) = z(L) = 0\}$. Now the weak formulation reads as follws: Find $(\theta, \tilde{w}) \in W_0(0,L)$ such that

$$\begin{aligned} \frac{h^3}{3}\int_0^L \psi\int_0^t \mathcal{M}(t-s)\ddot{\theta}(s)\mathrm{d}s + \frac{h^3}{3}\int_0^L \mathcal{D}\theta'\psi' - h\int_0^L \mathcal{G}(\tilde{w}' - \theta)\psi &= h\int_0^L \mathcal{G}\hat{w}'\psi \,, \\ h\int_0^L z\int_0^t \mathcal{N}(t-s)\ddot{\tilde{w}}(s)\mathrm{d}s + h\int_0^L \mathcal{G}(\tilde{w}' - \theta)z' &= \int_0^L zf(t,x) - h\int_0^L \mathcal{G}\hat{w}'z' \,, \end{aligned} \tag{38}$$

for all $(\psi, z) \in W_0(0, L)$. Then, the total deflection is $w(t,x) = \tilde{w}(t,x) + \overline{w}\frac{x}{L}(1 - \cos\omega t)$. Below we explain the time discretization of the time-convolution integrals. The discretization in space is done using the FE method.

3.2.1 Approximation of the convolution integral

Recalling the gentle start conditions, $\theta(0,x) = 0$, $\dot\theta(0,x) = 0$, we have

$$\int_0^t \sin[\alpha^r(t-s)]\ddot\theta(s)\mathrm{d}s = \alpha^r \int_0^t \cos[\alpha^r(t-s)]\dot\theta(s)\mathrm{d}s \ . \tag{39}$$

To approximate (39), we use the time docomposition $t = t - \Delta t + \Delta t$. Assuming θ is a real function, the folloing approximation is obtained ($\mathrm{i}^2 = -1$)

$$\begin{aligned}&\int_0^t \cos[\alpha^r(t-s)]\dot\theta(s)\mathrm{d}s \\ &\approx \cos(\alpha^r\Delta t)\Phi^r_\theta(t-\Delta t) - \sin(\alpha^r\Delta t)\Psi^r_\theta(t-\Delta t) + \cos\left(\alpha^r\frac{\Delta t}{2}\right)(\theta(t) - \theta(t-\Delta t)) \ ,\end{aligned} \tag{40}$$

where

$$\begin{aligned}\Phi^r_\theta(t) &= \int_0^t \cos[\alpha^r(t-s)]\dot\theta(s)\mathrm{d}s \ , \\ \Psi^r_\theta(t) &= \int_0^t \sin[\alpha^r(t-s)]\dot\theta(s)\mathrm{d}s \ .\end{aligned} \tag{41}$$

Differentiation in (41) yields the following coupled system of differential equations,

$$\begin{aligned}\dot\Phi^r_\theta(t) &= \dot\theta(t) - \alpha^r\Psi^r_\theta(t) \ , \\ \dot\Psi^r_\theta(t) &= \alpha^r\Phi^r_\theta(t) \ ,\end{aligned} \tag{42}$$

whereby $\Phi^r_\theta(0) = \Psi^r_\theta(0) = 0$. Equations (42) can be approximated by the fully implicit integration scheme; the following system of algebraic equations is obtained:

$$\begin{aligned}\Phi^r_\theta(t) + \Delta t\alpha^r\Psi^r_\theta(t) &= \theta(t) - \theta(t-\Delta t) + \Phi^r_\theta(t-\Delta t) \ , \\ -\Delta t\alpha^r\Phi^r_\theta(t) + \Psi^r_\theta(t) &= \Psi^r_\theta(t-\Delta t) \ .\end{aligned} \tag{43}$$

Thus, (40) with (43) constitutes a recurrent approximation of the convolution integral computed using the history integrals Φ^r_θ and Ψ^r_θ. The time convolutions associated with the deflection are treated in analogy; for the r-th mode we have

$$\begin{aligned}&\int_0^t \sin[\beta^r(t-s)]\ddot w(s)\mathrm{d}s = \\ &\approx \beta^r\left[\cos(\beta^r\Delta t)\Phi^r_w(t-\Delta t) - \sin(\beta^r\Delta t)\Psi^r_w(t-\Delta t) + \cos\left(\beta^r\frac{\Delta t}{2}\right)(w(t) - w(t-\Delta t))\right] \ ,\end{aligned} \tag{44}$$

where

$$\begin{aligned}\Phi^r_w(t) + \Delta t\beta^r\Psi^r_w(t) &= w(t) - w(t-\Delta t) + \Phi^r_w(t-\Delta t) \ , \\ -\Delta t\beta^r\Phi^r_w(t) + \Psi^r_w(t) &= \Psi^r_w(t-\Delta t) \ .\end{aligned} \tag{45}$$

We recall that the memory functions $\Phi^r_\bullet(t,x)$ and $\Psi^r_\bullet(t,x)$ are functions in time and space, as well as $\theta(t,x)$ and $w(t,x)$.

3.2.2 Time discretization of the phononic beam equation

Using the approximate expressions (40) and (44), the convolution integrals involved in the formulation (37) can be written, as follows (the abbreviation $\theta(t,\cdot)=\theta(t)$ is used),

$$\int_0^t \mathcal{M}(t-s)\ddot{\theta}(s,\cdot)\mathrm{d}s \approx \overline{\mathcal{M}}\ddot{\theta}(t,x) + \widetilde{\mathcal{A}}(t-\Delta t,x) + \widehat{\mathcal{M}}[\theta(t,x)-\theta(t-\Delta t,x)]\ , \tag{46}$$

where

$$\begin{aligned}\widetilde{\mathcal{A}}(t-\Delta t,x) &= \sum_r \alpha^r \widetilde{\mathcal{M}}^r \left(\cos(\alpha^r\Delta t)\Phi^r_\theta(t-\Delta t,x) - \sin(\alpha^r\Delta t)\Psi^r_\theta(t-\Delta t,x)\right)\ ,\\ \widehat{\mathcal{M}} &= \sum_r \alpha^r \widetilde{\mathcal{M}}^r \cos(\alpha^r\Delta t/2)\ .\end{aligned} \tag{47}$$

In analogy (and using the self-explaining notation) we obtain

$$\int_0^t \mathcal{N}(t-s)\ddot{w}(s,\cdot)\mathrm{d}s \approx \overline{\mathcal{N}}\ddot{w}(t,x) + \widetilde{\mathcal{B}}(t-\Delta t,x) + \widehat{\mathcal{N}}[w(t,x)-w(t-\Delta t,x)]\ , \tag{48}$$

where

$$\begin{aligned}\widetilde{\mathcal{B}}(t-\Delta t,x) &= \sum_r \beta^r \widetilde{\mathcal{N}}^r \left(\cos(\beta^r\Delta t)\Phi^r_w(t-\Delta t,x) - \sin(\beta^r\Delta t)\Psi^r_w(t-\Delta t,x)\right)\ ,\\ \hat{\mathcal{N}} &= \sum_r \beta^r \widetilde{\mathcal{N}}^r \cos(\beta^r\Delta t/2)\ .\end{aligned} \tag{49}$$

As can be seen from (46) and (48), it is necessary to approximate the second derivatives $\ddot{\theta}$ and $\ddot{w}$. We introduce the standard uniform time discretization of an interval $]0,T[$, such that $t_k = t_{k-1}+\Delta t$, $k=1,\ldots,\bar{k}$ with $t_0=0$ and $\Delta t = T/\bar{k}$. The time-discretized state variables $(\theta^k(x), w^k(x))$ are defined at time levels t_k, such that $\theta^k(x)\approx\theta(t_k,x)$ and $w^k(x)\approx w(t_k,x)$. The time convolutions can be approximated, as follows

$$\begin{aligned}\int_0^t \mathcal{M}(t-s)\ddot{\theta}(s)\mathrm{d}s &\approx \frac{1}{(\Delta t)^2}\left[(\overline{\mathcal{M}}+(\Delta t)^2\widehat{\mathcal{M}})\theta^k - (2\overline{\mathcal{M}}+(\Delta t)^2\widehat{\mathcal{M}})\theta^{k-1} + \overline{\mathcal{M}}\theta^{k-2}\right] + \widetilde{\mathcal{A}}^{k-1}\ ,\\ \int_0^t \mathcal{N}(t-s)\ddot{w}(s)\mathrm{d}s &\approx \frac{1}{(\Delta t)^2}\left[(\overline{\mathcal{N}}+(\Delta t)^2\widehat{\mathcal{N}})w^k - (2\overline{\mathcal{N}}+(\Delta t)^2\widehat{\mathcal{N}})w^{k-1} + \overline{\mathcal{N}}w^{k-2}\right] + \widetilde{\mathcal{B}}^{k-1}\ ,\end{aligned} \tag{50}$$

where $\widetilde{\mathcal{A}}^{k-1}$ and $\widetilde{\mathcal{B}}^{k-1}$ are approximations of $\widetilde{\mathcal{A}}(t_k-\Delta t,\cdot)$ and $\widetilde{\mathcal{B}}(t_k-\Delta t,\cdot)$, respectively.

Note, that the "pointwise in space" updates (43) and (45) can be defined simply for $t=t_k$ using the same equations.

3.3 Numerical illustration

In this section, we present examples of computations which are involved in numerical simulations of a phononic beam response in the time domain. The homogenized coefficients are computed, as described in Section 2.3.

For the circular inclusion, see Fig. 1, the resulting mass matrix convolution kernels for the Timoshenko beam model developed in Section 2.2 are depicted for a given time interval in Fig. 4. Two lowest frequency band-gap intervals are listed in Tab. 2, so that for any ω from these intervals one of the mass coefficients is negative, *i. e.* $M(\omega)<0$ or $N(\omega)<0$.

In the frequency, the following band gaps, i.e., intervals where $M(\omega)<0$ or $N(\omega)<0$, are present:

		λ [GPa]	μ [GPa]	ρ [kg/m^3]	γ
matrix:	aluminium	58.98	26.81	2799	5/6 μ
inclusions:	epoxy	1.79	1.48	1142	5/6 μ

Table 1: Material parameters on the micro-level, matrix-inclusion contrast $\approx 20\times 1$.

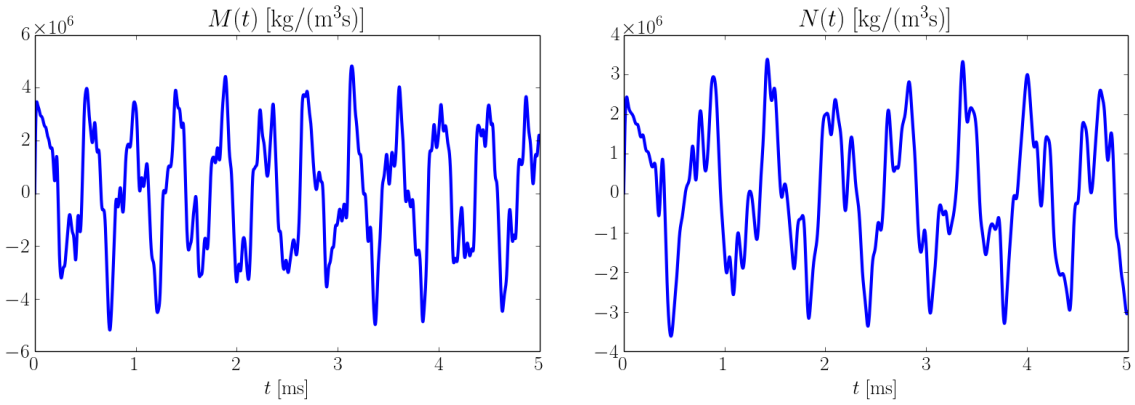

Figure 4: Illustration of the convolution kernels in the inertia terms of the phononic beam model.

coefficient	1st band gap [Hz]	2nd band gap [Hz]	
$M(\omega) < 0$ for	[14443, 14927],	[24093, 24190],	
$N(\omega) < 0$ for	[9698, 10042],	[22566, 22723],	

Table 2: The lowest frequency intervals, where $M(\omega) < 0$ or $N(\omega) < 0$, indicating a frequency band gap.

3.3.1 Approximation of convolution integrals

The numerical approximation of the convolution kernels associated with the beam deflections and rotations was described in previous sections. In Fig. 5, for the given function $\omega^2 \cos(\omega t)$ we compare the analytical and numerical computation of the convolutions

$$\int_0^t \mathcal{M}(t-s)\omega^2 \cos(\omega s)\mathrm{d}s \ , \quad \text{and} \quad \int_0^t \mathcal{N}(t-s)\omega^2 \cos(\omega s)\mathrm{d}s \ ,$$

are displayed as functions of t. For a better understading the relationship between the convolution result and the oscillating function with freqency ω of the function are displayed. The frequency $\omega = 10$ kHz is used, that lies in the band gap of $N(\omega)$, see Tab. 2.

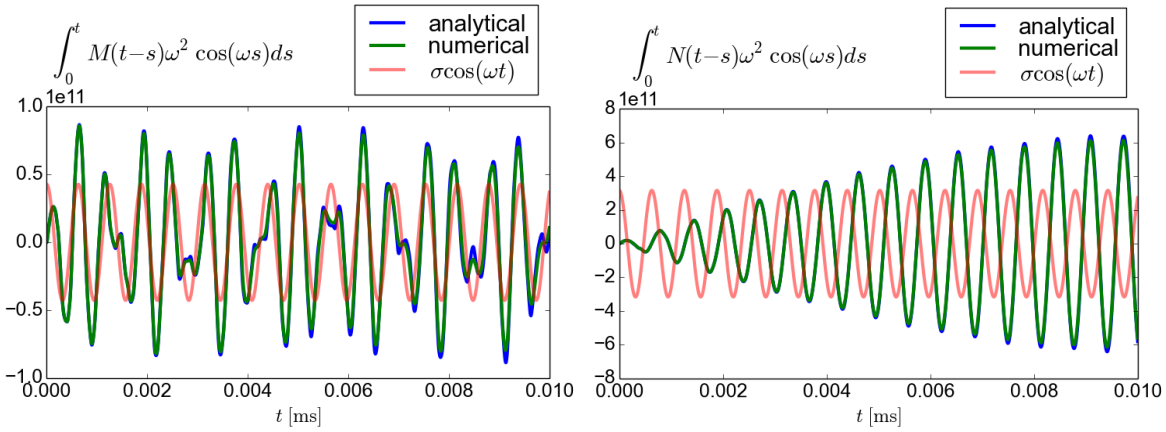

Figure 5: Illustrated accuracy of the convolution integrals evaluated numerically; comparison with an analytical evaluation for the function $\omega^2 \cos(\omega s)$, $\omega = 10kHz$ (the band gap of $N(\omega)$).

3.3.2 Wave response in the time domain

The weak formulation (38) was discretized in space by the finite element method. For the time discretization, the numerical scheme reported in Section 3 was employed the convolution integrals in time, as described above. In Fig. 6 we present results of one such calculation, for the loading frequency ω set to 9698 Hz, i.e. into the band-gap range of $\mathcal{N}(\omega)$ for the microstructure with the circular inclusion.

Qualitatively, we can see a damping of $w(t,x)$ waves coming from the periodic loading at $x = L$, which might be seen as the effect of $\mathcal{N}(\omega) < 0$ for the harmonic loading with frequency ω.

4 CONCLUSION

The aim of the paper was to present two methods for numerical modelling of dynamic behaviour of phononic structures described by the homogenized model developed in [2] and [6] using the two-scale homogenization of strongly heterogeneous elastic composites. The first method proposed in [4] relies on the spectral decomposition of the model equations in the frequency domain. For a given frequency of the harmonic loading, it allows to split the phononic structure response into two parts which are projected into two complementary Hilbert bases, one being associated with the positive mass, the other with the negative one. Due to this splitting we can compute the propagating part of the solution. Although we focused on the coupled

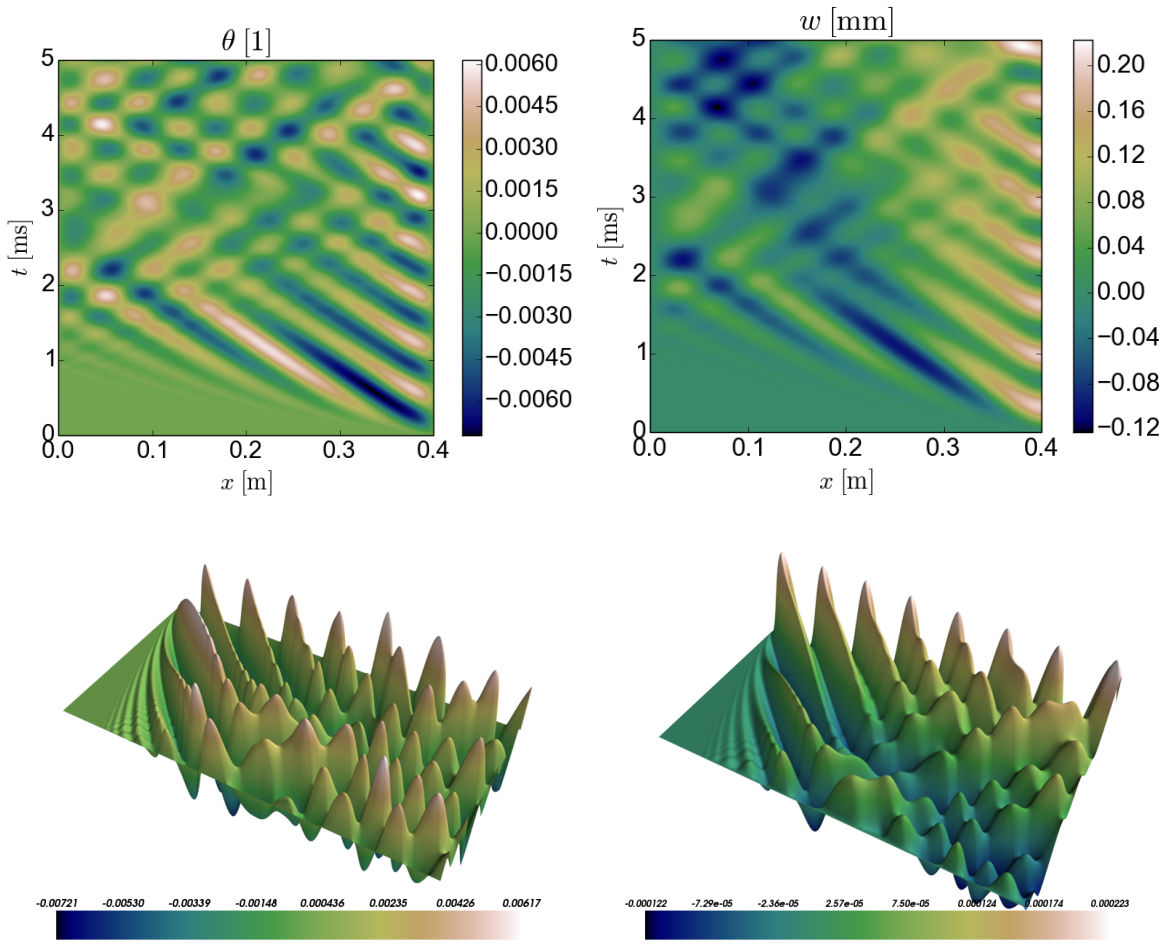

Figure 6: Wave propagation in the time domain, $\omega = 9698$ Hz. Top row: 2D view, bottom row: 3D view, left column: the rotation $\theta(t, x)$, right column: the deflection $w(t, x)$.

plate deflection and cross-sectional rotation wave propagation in plates or beams, this approach is rather general and can be applied to dynamic systems with indefinite coefficients of the terms corresponding to the inertia effects.

The second method relies on the elastodynamic problem formulation in the time domain, where the inertia terms are present in the form of time convolutions. We proposed a numerical discretization scheme which has been implemented in our FE code Sfepy and applied to simulate a wave response of the beam loaded kinematically with frequency in a partial band gap. Although the obtained result provide a comprehansive view of the partial band gap phenomenon, furher thesting and comporaison between the two approaches seems to be necessary for a deeper undersatnding the phononic structures response.

Acknowledgements The research and the participaton in the conference was supported in part by the grant project GACR 17-01618S and by the the project LO 1506 of the Czech Ministry of Education, Youth and Sports.

REFERENCES

[1] J. Auriault, C. Boutin, Long wavelength inner-resonance cut-off frequencies in elastic composite materials, *Int. Jour. Solids and Structures* **49**, 3269–3281, 2012.

[2] A. Ávila, G. Griso, B. Miara, E. Rohan, Multiscale modeling of elastic waves: Theoretical justification and numerical simulation of band gaps, *Multiscale Modeling & Simulation, SIAM*, **7**, 1–21, 2008.

[3] G. Milton, J. Willis, On modifications of Newton's second law and linear continuum elastodynamics, *Proc. R. Soc. A*, **483**, 855–880, 2007.

[4] E. Rohan, R. Cimrman, and B. Miara. Modelling response of phononic Reissner-Mindlin plates using a spectral decomposition. *Applied Mathematics and Computation*, **258**, 617–630, 2015.

[5] E. Rohan, B. Miara, Sensitivity analysis of acoustic wave propagation in strongly heterogeneous piezoelectric composite, *in: Topics on Mathematics for Smart Systems*, (World Sci. Publishing Company), 139–207, 2006.

[6] E. Rohan, B. Miara, Elastic waves in strongly heterogeneous periodic plates of the Reissner-Mindlin and Kirchhoff-Love types. *ZAMM - Journal of Applied Mathematics and Mechanics*, **96**, 304–326, 2016.

[7] E. Rohan, B. Miara, and F. Seifrt. Numerical simulation of acoustic band gaps in homogenized elastic composites. *International Journal of Engineering Science*, **47**, 573–594, 2009.

[8] V. P. Smyshlyaev, Propagation and localization of elastic waves in highly anisotropic periodic composites via two-scale homogenization, *Mechanics of Materials*, **41**, 434–447, 2009.

[9] J. Vondřejc, E. Rohan, J. Heczko, Shape optimization of phononic band-gap structures using the homogenization approach. *Int. Jour. Solids and Structures*, on-line (http://dx.doi.org/10.1016/j.ijsolstr.2017.01.038), 2017

[10] T. Wu, J. Hsu, J. Sun, Phononic plate waves, IEEE Transactions on Ultrasonics, Ferroelectrics, and Frequency Control **58**, 2146–2161, 2011.